Cancer Management and Research

Elevate Series

Open Access Full Text Article

ORIGINAL RESEARCH

Inhibitory Effects of Paclitaxel-Loaded Iron Oxide Nanoparticles on Non-Small Cell Lung Cancer by Enhancing Autophagy-Dependent Ferroptosis and Apoptosis Pathways

Rongchu Deng[1,*], Guanghong Liang[1,*], Wenqing Chen[1,2], Qi Nie[1], Jian Wen[1]

[1]Department of Guangxi Clinical Research Center for Neurological Diseases, The Affiliated Hospital of Guilin Medical University, Guilin, Guangxi, People's Republic of China; [2]College of Pharmacy, Guilin Medical University, Guilin, Guangxi, People's Republic of China

*These authors contributed equally to this work

Correspondence: Jian Wen, Department of Guangxi Clinical Research Center for Neurological Diseases, The Affiliated Hospital of Guilin Medical University, Guilin, Guangxi, People's Republic of China, Email wenjian2400@163.com

Background: Iron oxide nanoparticles coated with paclitaxel (IONP@PTX) are frequently applied to various tumor types. However, inhibitory effect and possible mechanism of IONP@ PTX on non-small-cell lung cancer (NSCLC) remain unclear.

Objective: This work aimed to assess inhibitory effects and potential mechanisms of IONP@PTX on lung cancer A549 cells and further explore the nanomedicine delivery systems for applications in cancer therapies.

Methods: Morphology features and qualities of IONP@PTX were directly assessed. After treatment of A549 cells with either PTX or IONP@PTX, cell viability and apoptosis were separately detected by CCK-8 assay and flow cytometry. In addition, intracellular iron ion, lipid peroxidation (LPD) and reactive oxygen species (ROS) were identified by using an iron colorimetric assay kit, DCFH-DA and C11-BODIPY fluorescent probe, respectively. Moreover, the expression levels of autophagy-, ferroptosis-, and apoptosis-related proteins were measured by Western blot.

Results: The synthesized IONP@PTX had a core particle size of about 10 nm and a hydrated particle size of 31.01±2.47 nm. In comparison with PTX, IONP@PTX had a stronger anti-tumor effect on A549 cells, with considerably higher levels of ROS, LPD, and total iron ion concentration ($P<0.05$). Likewise, IONP@PTX markedly reduced the expression levels of GPX4, FTH, and SLC7A11 proteins whereas obviously increased the expression levels of LC3II/I and ACSL4 proteins ($P<0.05$). Furthermore, the inhibitory effects of both PTX and IONP@PTX on A549 cells could be evidently reversed by additional 3-methyladenine (3-MA) or ferrostatin-1. Interestingly, the apoptosis rates of A549 cells, together with the expression level of pro-apoptotic protein Cleaved caspase-3, were significantly higher in the IONP@PTX group than those in the control and PTX groups ($P<0.05$).

Conclusion: IONP@PTX inhibits the proliferation of human lung cancer A549 cells by enhancing autophagy-dependent ferroptosis and apoptosis pathways.

Keywords: IONP@ PTX, paclitaxel, ferroptosis, autophagy, apoptosis

Introduction

Lung cancer is one of the most prevalent causes of morbidity and mortality in both men and women across the globe,[1] in which non-small cell lung cancer (NSCLC) accounts for up to 85% of instances, making it the second most frequent malignant tumor in the world, with the greatest incidence and fatality rate.[2] Given that most individuals suffering from NSCLC do not exhibit noticeable symptoms during the early stages, more than 55% of patients have many metastases prior to diagnosis,[3] with the brain being the most common site of distant metastases from NSCLC, responsible for 20% ~ 65% lung cancer cases. This is a much greater prevalence of brain metastases from lung cancer than from melanoma, breast, kidney, and colorectal cancers.[4] NSCLC patients with brain metastases have very poor prognosis and significant impairments to their quality of life, survival rate, and cognitive function. Worse still, even after receiving treatment, patients face risks and difficulties such as poor long-term survival rates, low sensitivity to chemotherapy drugs, and high

Received: 21 September 2024
Accepted: 17 January 2025
Published: 11 March 2025

rates of metastasis and recurrence following surgery. Thus, novel approaches to suppress the development and spread of NSCLC are required.

Paclitaxel (PTX), which is extracted as an active component from recently harvested Picea abies plants, has been approved as a novel medication by the Food and Drug Administration (FDA) for more than thirty years.[5] As one of the chemotherapeutic agents with a high frequency of clinical use, PTX is currently used widely in the treatment of malignant tumors including breast cancer, ovarian cancer, NSCLC, pancreatic cancer, esophageal cancer, gastric cancer, head and neck tumors, soft tissue sarcoma, and others.[6,7] As the cornerstone of chemotherapy treatments, PTX contributes to the induction of microtubule protein polymerization, preventing tumor cells from reproducing and ultimately leading to cell apoptosis by causing cell cycle arrest at the G2/M phase indefinitely.[8,9] However, the antitumor efficaciousness of PTX may be somewhat impacted by its biological properties, including low bioavailability, poor water solubility, and high incidence of toxicity. Clinically, some adverse reactions, including hepatotoxicity, alopecia, myelosuppression, neurotoxicity, cardiovascular toxicity, joint and muscle pain, and gastrointestinal reactions, result from PTX.[10] To mitigate these disadvantages, a number of innovative drug delivery systems, including liposomes, polymeric micelles, nanoemulsions, nanosuspensions, and nanoparticles, has been developed, at least in part, to improve the targeted cellular administration of PTX.[10–12]

The nanoparticle is a synthetic, minuscule particle with a size of up to 100 nanometers, and it could take the shape of carbon particles, metal particles, ceramic particles, emulsions, or polymers. Nowadays, nanoparticles have been the focus of a growing body of research due to their special characteristics, such as their nanosize, biocompatibility, high surface-to-volume ratio, and ease of surface modification.[13] The discovery of nanomaterial-mediated medications represents a major therapeutic advance in anticancer treatment. The reason is that therapeutic medications are not rapidly removed from the body thanks to nanoparticles, which not only efficiently control drug release and attenuate drug toxicity, but also boost immunity against microorganisms, consequently enhancing therapeutic efficacy and lessening the adverse effects of drugs on the body.

An increasing number of researches have demonstrated the anti-tumor effects of PTX in conjunction with nanoparticles on their enhanced performance. Our previous study has confirmed that iron oxide nanoparticles loaded with PTX (IONP@PTX) have been shown great potential in treating various tumor types.[13,14] Recently, a randomized, open-label, noninferiority Phase 3 trial has reported that patients receiving albumin-conjugated PTX have good overall survival, progression-free survival, and objective response rate regardless of the histologic type. These data suggest that the medication regimen thought to be a potential treatment modality has a potent therapeutic effect on patients with advanced NSCLC.[15,16] Similarly, polymeric lipid nanoparticles have been demonstrated effectively and efficiently to deliver tonic calcitonin to the targeted tumors and facilitate PTX-mediated toxicity and apoptosis of MDA-MB-231 cells, showing a notable capacity to impede cell migration and invasive activity via linking to IRAK1 and NF-κB expression. All of these data imply a significant enhancement in the therapeutic efficacy of PTX in metastatic breast cancer.[17] More recently, an in vitro and in vivo investigation demonstrates an enhanced efficacy of nanoparticle albumin-bound PTX for human lung and colorectal cancers via sequestosome 1-mediated nanodrug delivery.[18]

With the rapid development of nanodrug loading technology, it is possible to alter the pattern of tumor cell death as well as its essential variations and immunogenicity requirements.[19,20] Ferroptosis, a recently identified form of programmed cell death, is characterized by the build-up of lipid peroxides and the iron-dependent, non-enzymatic inactivation of the lipid hydroperoxidase glutathione peroxidase 4 (GPX4).[21,22] Contrary to apoptosis, cysteine proteases, apoptosis-associated proteins, and mitochondrial damage are not necessary for occurrence of ferroptosis, during which reactive oxygen species (ROS) or glutathione (GSH) deficiency can cause a number of signaling mechanisms, such as lipid-soluble antioxidants, electrophilic medications, and specific toxicants.[23,24]

Autophagy is a lysosome-mediated degradation system that plays a crucial role in cellular homeostasis through the degradation of cytoplasmic components, such as eliminating damaged organelles, breaking down aging or aberrant proteins, controlling cell cycle, and triggering cell death. It is therefore of great importance for the survival and well-being of cells, which are involved in the development of many illnesses, including cancer, neurological disorders, and metabolic disorders.[25]

Herein, our present study aimed to assess the inhibitory effects and potential mechanisms of IONP@PTX on lung cancer A549 cells and further explore the nanomedicine delivery systems for applications in cancer therapies.

Materials and Methods

Preparation of IONP@PTX

IONP@PTX was synthesized according to our previously reported procedures.[13,14] Thereafter, zeta potential, hydrated particle size, and nanoparticle size properties of IONP@PTX were separately determined by using a nanoparticle size and zeta potential analyzer (Malvern Panalytical Ltd. UK, model Zetasizer Lab) and transmission electron microscopy (HITACHI, model HT7800). In addition, the stability of IONP@PTX was dissolved in diluted pure water and determined the hydrodynamic size versus zeta potential of IONP@PTX over a period of 5 weeks by colloidal stability analysis.

Moreover, drug loading and release were determined by spectral analysis with a UV-visible spectrophotometer (UV-1780; Shimadzu, Japan). Briefly, different concentrations of PTX (0.5, 4.0, 8.0, 16.0, 32.0, and 64.0 μg/mL) were analyzed by high performance liquid chromatography (LC-15C; Shimadzu, Japan) in order to establish a standard curve at 227 nm as $y = 36275x + 28659$ ($R^2 = 0.9988$) and further to calculate the concentration by the following formula: Loading of PTX/mg (Fe concentration) solution: Loading capacity= concentration × dilution × volume.

Cell Culture

A549 cells were supplied by Jiangsu KGI Biotechnology Co., Ltd. and cultured in 90% F12K medium supplied with 10% fetal bovine serum (FBS) and 1% penicillin and streptomycin in an incubator at 37°C with 5% CO_2 and saturated humidity (Thermo Fisher Scientific, Inc).

Cell Viability

After 24 hour-incubation of the A549 cells with different concentrations of IONP@PTX and PTX (0, 0.1, 0.2, 0.4, 0.6, 0.8, 1.0, 1.2, 2.4, and 3.6 μg/mL), respectively, the cell viability was determined according to the manufacturer's instructions by CCK-8 (cat.no. CP736; DOJINDO Laboratories, Japan) assay. Briefly, the cells were digested with 0.25% trypsin (without EDTA), counted, and prepared for a cell suspension at a concentration of 8×10^4 cells/mL. Thereafter, 100 μL cell suspension was seeded in each well of a 96-well cell culture plate at 37 °C, 5% CO_2 incubator for 24 hours, and then 100 μL corresponding drug containing medium at different concentrations was added to each well. Meanwhile, a negative control group was set up. After 24 hour-incubation again, the optical density (OD) of each well was measured at 450 nm on microplate reader (TECAN SPARK, Switzerland).

Cell Apoptosis

A549 cells were divided into 9 groups, namely 0 μg/mL PTX (Control group), 0.8 μg/mL PTX (PTX group), 0.8 μg/mL IONP@PTX (IONP@PTX group), 2 μM ferrostatin-1 (ferrostatin-1 group), 0.8 μg/mL PTX+ 2 μM ferrostatin-1 (PTX+ ferrostatin-1 group), 0.8 μg/mL IONP@PTX+2 μM ferrostatin-1 (IONP@PTX+ ferrostatin-1 group), 5 mM 3-MA (3-MA group), 0.8 μg/mL PTX+5 mM 3-MA (PTX+ 3-MA group), and 0.8 μg/mL IONP@PTX+5 mM 3-MA (IONP@PTX +3-MA). After incubation for 24 hours, the cells were digested, washed twice with PBS (cat.no. KGB5001; Jiangsu Kaiji Biotechnology Co., Ltd.), and collected by centrifugation. Then, 1×10^6/mL cells were suspended in 500 μL binding buffer, added with 5 μL Annexin V-APC (KGA1024) and 5 μL 7-aminoactinomycin D (7-AAD), mixed, and kept at room temperature in the dark for 5~15 minutes. Finally, cell apoptosis was detected by flow cytometry (BECKMAN COULTER CytoFLEX). In each panel, the lower left quadrant and upper left quadrant separately indicate the percentage of live cells (LL) and the percentage of dead cells (UL), and the lower right quadrant and the upper right quadrant represent the percentage of early apoptotic cells (LR) and the percentage of late apoptotic cells (UR), respectively. And the percentage of early apoptotic cells plus late apoptotic cells represents for the apoptosis rate.

Detection of Iron Ion

Total iron ion concentration was quantified by an iron colorimetric assay kit (cat.no. E-BC-K881-MElabscience). After treatment of A549 cells as above mentioned, 1×10^6 cells/mL were resuspended with 0.2 mL PBS and then lysed on the ice box for 10 minutes. After centrifugation at 15,000 × g for 10 minutes, the supernatant was taken as a backup. Then, 80 μL standard

products in different mass concentrations were added into the corresponding wells of the enzyme plate as standard wells, 80 μL samples to be tested were added into the assay wells, and 80 μL control solution was added into the control wells. After adding 80 μL color development solution into the assay wells and standard wells of a 96-well plate, it was mixed gently and incubated at 37 °C for 10 minutes. Finally, the OD of each well was measured at the length of 593 nm on a microplate reader (TECAN SPARK, Switzerland).

Detection of Intracellular ROS

First, cells were digested, counted, and prepared into a cell suspension with a concentration of 5×10^4 cells/mL. Then, 500 μL of the cell suspension was added to each well in a 24-well cell culture plate, and the cells were allowed to attach to the wall after incubation overnight. According to the experimental groups, each well was subsequently changed to 500 μL of the corresponding drug-containing medium and treated for 24 hours. After treatment, discard the supernatant, wash with PBS for 3 times, and then discard PBS. Following this, an appropriate amount of DCFH-DA (Jiangsu Kaiji Biotechnology Co., Ltd.) working liquid, diluted 1:1,000 with serum-free culture medium to a final concentration of 10 μM, was added to each well. The probe and cells were then allowed to fully contact in the cell incubator at 37°C for 20 minutes. Next, an appropriate amount of Hoechst 33342 (Jiangsu Kaiji Biotechnology Co., Ltd.) staining solution (1:1,000 dilution) was added to each well, and the plate was placed at room temperature for 10 minutes in the dark. The supernatant was discarded again, and the cells were washed with PBS three more times. Finally, the cells were observed and photographed under a microscope (IX51; OLYMPUS, Japan) at 200 times magnification. See Supplementary material for the detailed process of ROS determination.

Detection of Lipid Peroxidation (LPD)

First, cells were digested, counted, and prepared into a cell suspension with a concentration of 5×10^4 cells/mL. Then, 500 μL of the cell suspension was added to each well in a 24-well cell culture plate, and the cells were allowed to attach to the wall after incubation overnight. According to the experimental groups, each well was subsequently changed to 500 μL of the corresponding drug-containing medium and treated for 24 hours. After treatment, an appropriate amount of BODIPY^{TM} (cat. no. D3861;Thermo Fisher Scientific, Inc.) staining solution diluted with serum-free culture solution at 1:1,000 was added to each well to make the probe fully contact with the cells, and the probe was placed at room temperature for 20 minutes away from light. The probe and cells were then allowed to fully contact in the cell incubator at 37°C for 20 minutes. Next, an appropriate amount of Hoechst 33342 (cat.no. KGA212-1; Jiangsu Kaiji Biotechnology Co., Ltd.) staining solution (1:1,000 dilution) was added to each well, and the plate was placed at room temperature for 10 minutes in the dark. The supernatant was discarded again, and the cells were washed with PBS three more times. Finally, the cells were observed and photographed under a microscope (IX51; OLYMPUS, Japan) at 200 times magnification. See Supplementary material for the detailed process of LPD determination.

Western Blot

The pretreated cells were homogenized in lysis buffer, separated by 10% sodium dodecyl sulfate polyacrylamide gel electrophoresis, and transferred to nitrocellulose membrane (Shanghai Epizyme Biomedical Technology Co., Ltd.). The membrane was blocked with 5% skimmed milk, washed three times with TBST for 10 minutes, and then incubated with diluted primary rabbit antibodies, including anti-SLC7A11 (1:1,000, Affinity DF2509), anti-FTH (1:1,000, abcam ab5972), anti-GPX4 (1:6,000, Abcam ab5066), anti-ACSL4 (1:30,000, Abcam ab5282), anti-Beclin1 (1:1,000, Abcam ab2557), anti-Bcl2 (1:2,000, Abcam ab2858), anti-Cleaved caspase-3 (1:500, abcam ab2042), anti-LC3 II/I (1:1,000, abcam ab8394), anti-β-actin (1:1,000, cat.no.KGAA006; Jiangsu Kaiji Biotechnology Co., Ltd.). After washing three times with TBST for 10 minutes, the membrane was incubated with goat anti-rabbit IgG-HRP (cat.no. KGAA35; Jiangsu Kaiji Biotechnology Co., Ltd.) for 1 hour. Thereafter, the proteins were visualized using an enhanced chemiluminescent detection kit (Shanghai Epizyme Biomedical Technology Co., Ltd.). β-actin was served as normalize protein levels.

Statistical Analysis

Statistical analysis was performed using GraphPad Prism 9.0.5 software (GraphPad Software; Dotmatics). All data were based on at least three replicate experiments. If the data conformed to a normal distribution, they were expressed as mean

± standard deviation and analyzed using a one-way ANOVA. On the contrary, they were expressed as medians (quartiles) and the Kruskal–Wallis *H*-test was used, following with Tukey post hoc tests. A two-sided $P<0.05$ was considered to be statistically significant difference.

Results

Characterization of IONP@PTX

Under transmission electron microscopy, the synthesized IONP@PTX was uniformly distributed and well dispersed, with a core particle size of about 10 nm, a hydrated particle size of 31.01 ± 2.47 nm, and a zeta potential of −48.28 ± 4.89 mV (Figure 1A, B and C). UV-visible spectrophotometric detection showed that the full band scanning of IONP@PTX solution ranged from 200 to 1,000 nm (Figure 1D), with a high absorption peak at 227 nm. The standard curve of PTX was developed by high-performance liquid chromatography and the peak area was 1,387,098, with an encapsulation rate of 74.9% and drug loading of 25.84% (Figure 1E). Moreover, stability assay confirmed no significant changes of particle size and zeta potential in five weeks (Figure 1F and G), implying a stable of IONP@PTX.

Impact of PTX and IONP@PTX on Cell Viability

After treatment of A549 cells for 24 hours, the cell viability declined with the increasing concentrations of both IONP@PTX and PTX in comparison to 0 μg/mL either IONP@PTX or PTX. This suggests that both PTX and IONP@PTX suppress the viability of NCLC A549 cells in a dose-dependent manner. When the concentration of IONP@PTX and PTX reached to 0.8 μg/mL, IONP@PTX had a much stronger inhibitory effect on A549 cells than PTX ($P<0.05$) (Figure 2), showing a significant difference between them.

Effect of IONP@PTX on Induction of Ferroptosis in A549 Cells

After A549 cells were separately co-incubated with PTX and IONP@PTX for 24 hours, IONP@PTX significantly increased the total iron ion concentration, intracellular ROS, and LPD levels ($P<0.05$, Figure 3A–C), and markedly upregulated the expression level of acyl-CoA synthetase long chain family member 4 (ACSL4) protein, while

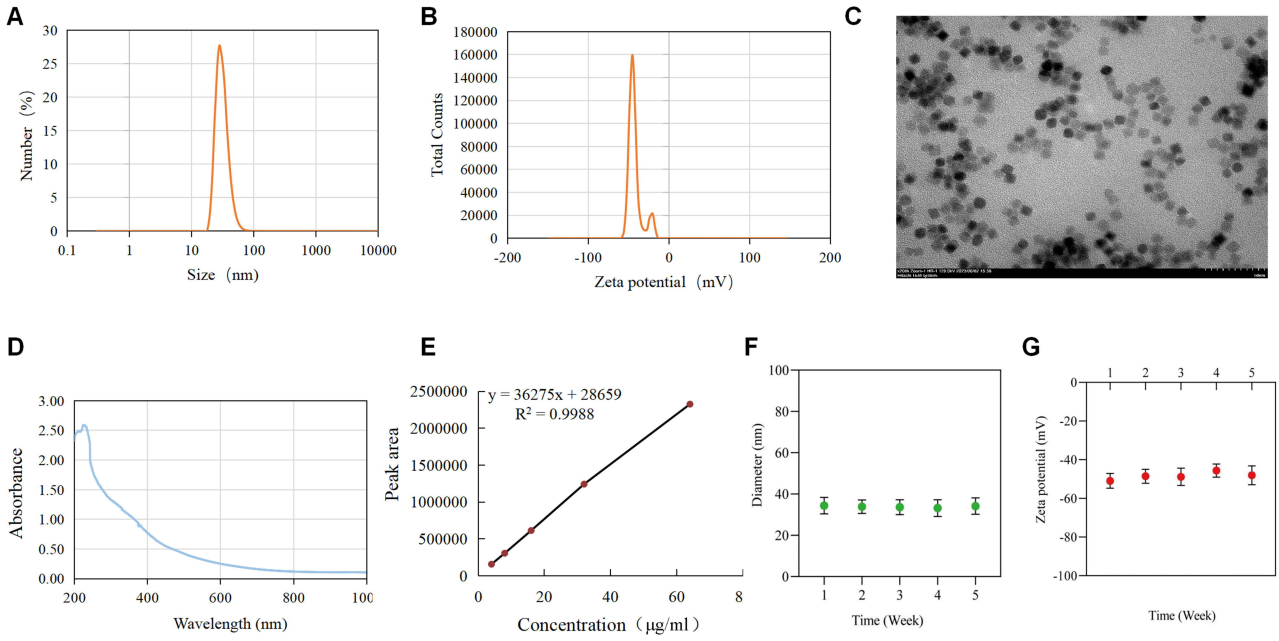

Figure 1 Characterization of IONP@PTX. (**A**) Average particle size of IONP@PTX; (**B**) Zeta potential of IONP@PTX; (**C**) Image of IONP@PTX under transmission electron microscopy (scale bar: 50 nm); (**D**) UV absorption spectra analysis of IONP@PTX; (**E**) Standard curve of PTX; (**F**) Stability assay of IONP@PTX; (**G**) Zeta potential of IONP@PTX.

Abbreviations: IONP, iron oxide nanoparticles; PTX, paclitaxel; TEM, transmission electron microscopy.

https://doi.org/10.2147/CMAR.S497238

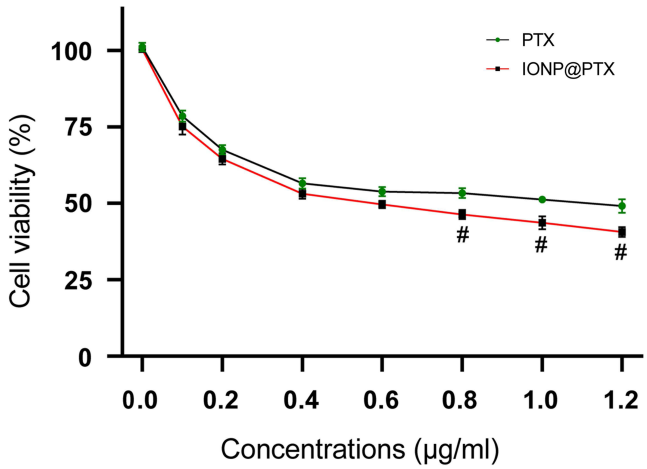

Figure 2 Effect of IONP@PTX and PTX on A549 cell viability. $^{\#}P < 0.05$, compared with the same concentration of PTX.
Abbreviations: IONP, iron oxide nanoparticles; PTX, paclitaxel.

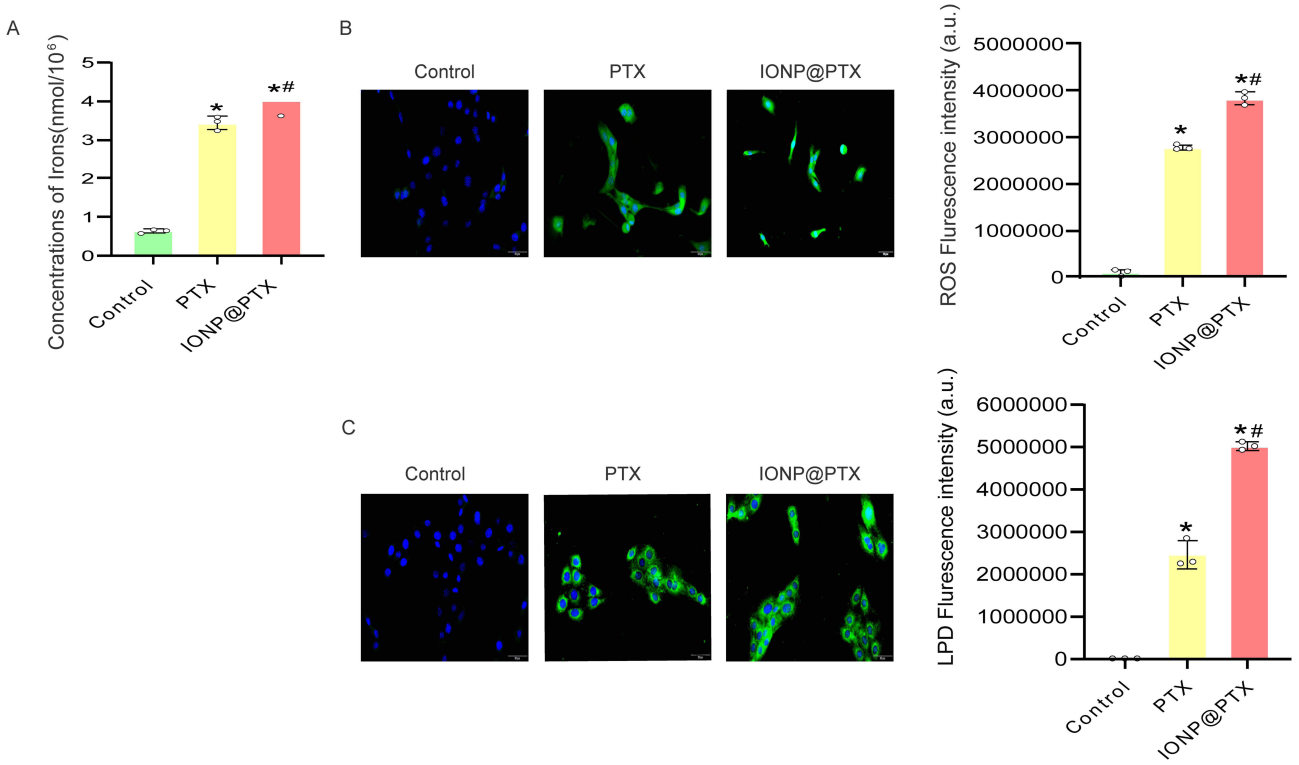

Figure 3 Effect of IONP@PTX on induction of ferroptosis in A549 cells. (**A**)Total iron ion concentration; (**B**) Representative images of A549 cells after staining with DCFH-DA (Magnification: 200×) and relative intracellular levels of ROS; (**C**) Representative images of A549 cells after staining with BODIPYTM (Magnification: 200×) and relative intracellular levels of LPD. $^{*}P < 0.05$, compared with control group; $^{\#}P < 0.05$, compared with the PTX group.
Abbreviations: IONP, iron oxide nanoparticles; PTX, paclitaxel; ROS, reactive oxygen species; LPD, lipid peroxidation.

downregulating the levels of GPX4, ferritin heavy chain (FTH), and solute carrier family 7 member 11 (SLC7A11) proteins ($P<0.05$, Figure 4A and B). All these data suggest that ferroptosis in A549 cells is triggered by IONP@PTX.

Reversal of IONP@PTX-Induced Ferroptosis by Ferrostatin-1

After co-incubation of A549 cells with PTX, IONP@PTX, ferrostatin-1, a combination of PTX with ferrostatin-1, and a combination of IONP@PTX with ferrostatin-1 for 24 hours, total iron ion concentration, intracellular levels of ROS

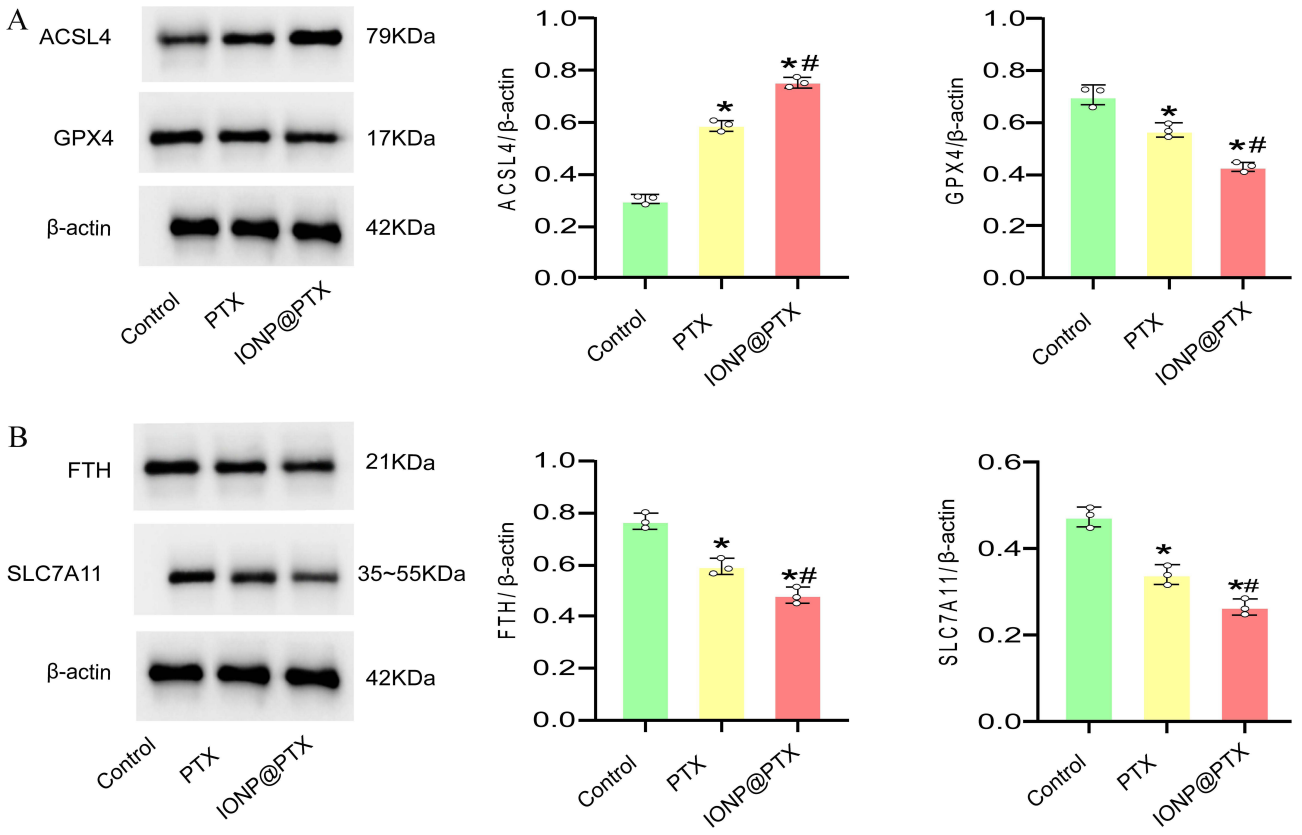

Figure 4 Determination of proteins in A549 cells by Western blot. (**A**)Relative expression levels of ACSL4 protein and relative expression levels of GPX4 protein; (**B**) Relative expression levels of FTH protein and relative expression levels of SLC7A11 protein. Error lines were from triplicate runs. *$P < 0.05$, compared with the control group; #$P < 0.05$, compared with the PTX group.
Abbreviations: IONP, iron oxide nanoparticles; PTX, paclitaxel.

and LPD were significantly higher in the IONP@PTX group compared with either PTX or control groups ($P<0.05$) (Figure 5A–C. Additionally, the expression level of FTH protein in the IONP@PTX group was significantly lower than that of control group ($P<0.05$), and slightly lower than that of the PTX group ($P>0.05$) (Figure 6A), whereas that of Light Chain 3 (LC3) II/I protein was significantly higher in the IONP@PTX group compared with either PTX or control groups ($P<0.05$) (Figure 6B). Interestingly, the inhibitory effects of PTX and IONP@PTX were lessened by the ferroptosis inhibitor ferrostatin-1 (Figure 5A–C and Figure 6A and B). Accordingly, ferrostatin-1 inhibits the iron mortality in A549 cells caused by IONP@PTX.

IONP@PTX-Induced Ferroptosis in A549 Cells via the Autophagy Pathway

After A549 cells were separately co-incubated with PTX, IONP@PTX, 3-MA, a combination of PTX with 3-MA, and a combination of IONP@PTX with 3-MA for 24 hours, total iron ion concentration, ROS, and lipid peroxidation increased significantly in the IONP@PTX group compared with PTX group and control group ($P<0.05$; Figure 7A–C). Simultaneously, expression levels of LC3II/I and Beclin1 proteins were significantly higher in the IONP@PTX group compared with control group and PTX group ($P<0.05$; Figure 8A and B).The level of FTH protein was significantly lower than that of the control group ($P<0.05$), and slightly lower than that of the PTX group ($P>0.05$; Figure 8B).This suggests that IONP@PTX induces autophagy in A549 cells.

It is worth noting that when the additional autophagy inhibitor 3-MA was used in combination with PTX or IONP@PTX, compared with the corresponding PTX and IONP@PTX, the total iron ion concentration, ROS, lipid peroxidation, and the level of LC3II/I protein were all reduced (all $P<0.05$; Figures 7A–C, and 8B), while the level of FTH protein was significantly increased ($P<0.05$; Figure 8B). These findings imply that the initiation of ferroptosis is triggered by upregulating the autophagy pathway, which can be reversed by the autophagy inhibitor 3-MA.

https://doi.org/10.2147/CMAR.S497238

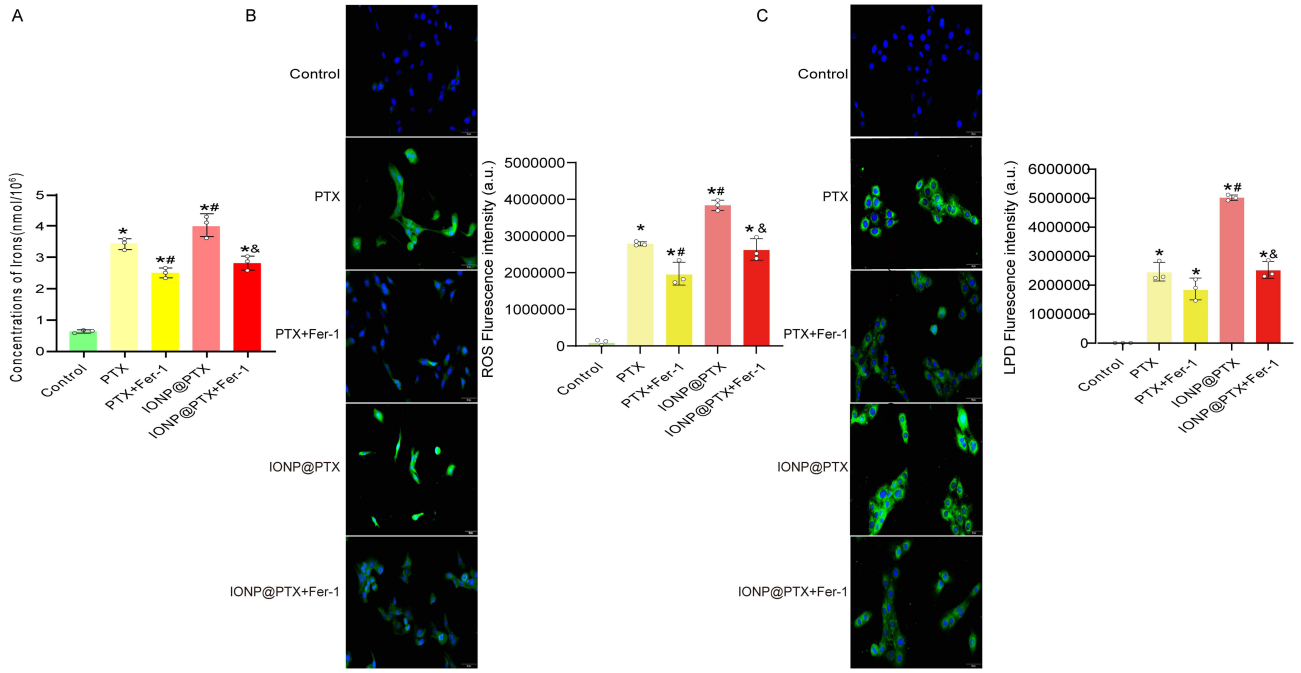

Figure 5 Reversal of IONP@PTX-induced ferroptosis by ferrostatin-1. (**A**) Total iron ion concentration; (**B**) Intracellular levels of ROS *(Magnification: 200×)*; (**C**) Intracellular levels of LPD (Magnification: 200×); Error lines are were from triplicate runs. **P* < 0.05, compared with control; **P* < 0.05, compared with control; $^{\#}P$ < 0.05, compared with PTX group; $^{\&}P$ < 0.05, compared with IONP@PTX group.
Abbreviations: IONP, iron oxide nanoparticles; PTX, paclitaxel; ROS, reactive oxygen species; LPD, lipid peroxidation; Fer-1, ferrostatin-1.

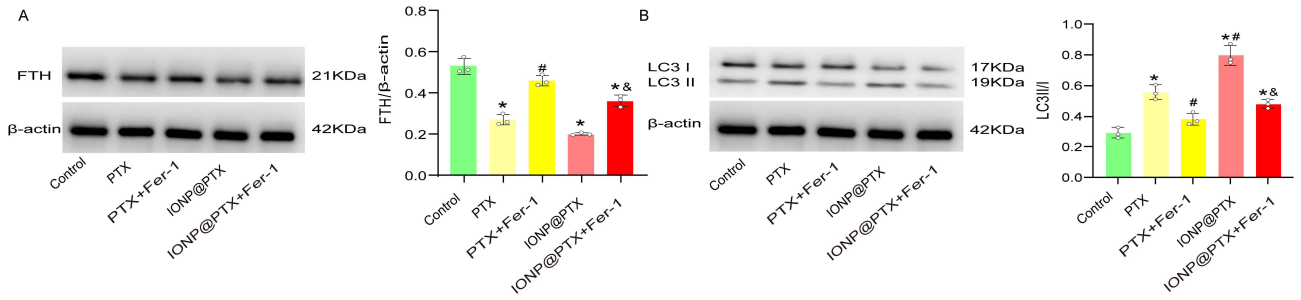

Figure 6 Determination of FTH and LC3II/I-related proteins by Western blot. (**A**) Representative images and relative expression of FTH proteins in A549 cells treated with or without additional ferrostatin-1; (**B**) Representative images and relative expression of LC3II/I-related proteins in A549 cells treated with or without additional ferrostatin-1; Error lines were from triplicate runs. **P* < 0.05, compared with control; $^{\#}P$ < 0.05, compared with PTX group; $^{\&}P$ < 0.05, compared with IONP@PTX group.
Abbreviations: IONP, iron oxide nanoparticles; PTX, paclitaxel;Fer-1.ferrostain-1.

IONP@PTX-Induces Apoptosis via the Autophagy Pathway to Achieve Anti-Tumor Effects

After 24 hour-co-incubation with PTX, IONP@PTX, 3-MA, ferrostatin-1, a combination of PTX with 3-MA, a combination of IONP@PTX with 3-MA, a combination of PTX with ferrostatin-1, and a combination of IONP@PTX with ferrostatin-1, the apoptosis rate of A549 cells in the IONP@PTX group was significantly higher compared with the control and PTX groups (all $P<0.05$) (Figure 9A–C). And the expression level of pro-apoptotic protein Cleaved caspase-3 were higher in the IONP@PTX group compared with the control group and PTX group ($P<0.05$) (Figure 10A–C). Of note, the additional autophagy inhibitor 3-MA or ferroptosis inhibitor ferrostatin-1 impaired the effects of PTX and IONP@PTX on the cell apoptosis and the expression of apoptosis-related protein ($P<0.05$; Figures 9B, C and 10B, C). Accordingly, it is postulated that IONP@PTX induces cell apoptosis via the autophagy-dependent ferroptosis driven by ROS.

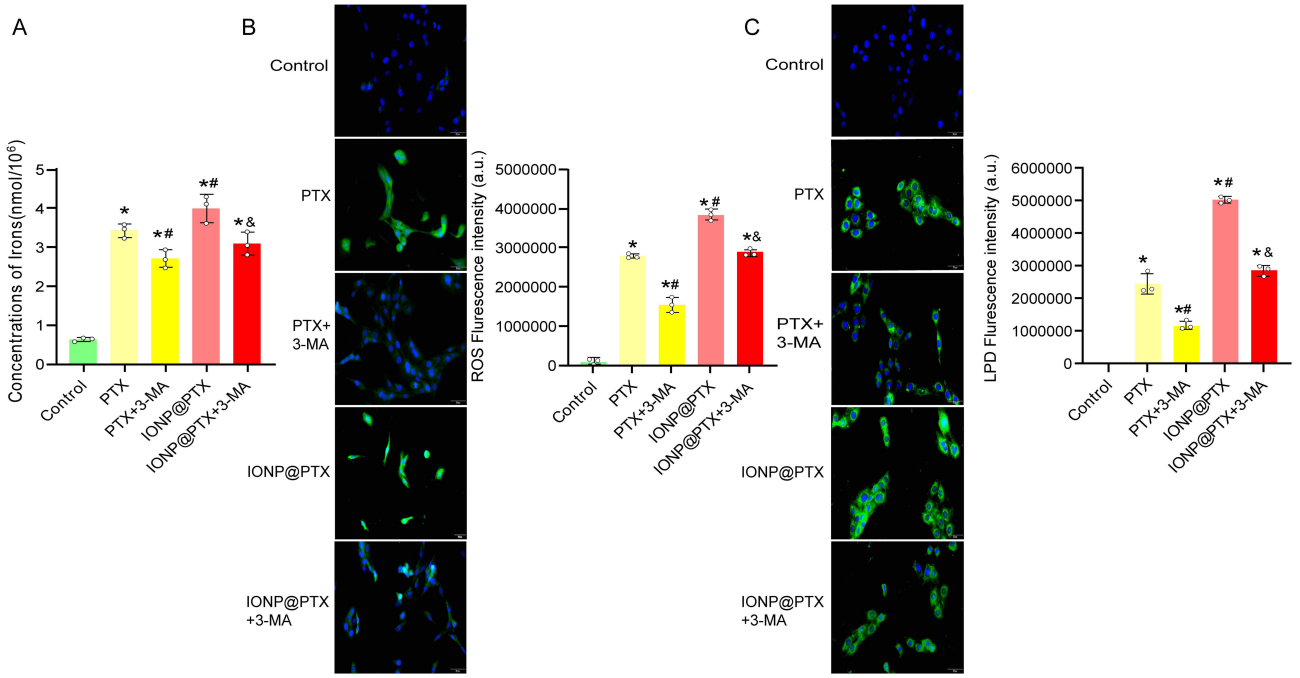

Figure 7 Reversal of IONP@PTX-induced autophagy ferroptosis in A549 cells by additional 3-MA. (**A**)Total iron ion concentration; (**B**) Intracellular ROS levels; (**C**) Intracellular lipid peroxidation. Error lines were from triplicate runs. *P < 0.05, compared with control group; #P < 0.05, compared with PTX group; &P < 0.05, compared with IONP@PTX group.

Abbreviations: IONP, iron oxide nanoparticles; PTX, paclitaxel; 3-MA, 3-methyladenine.

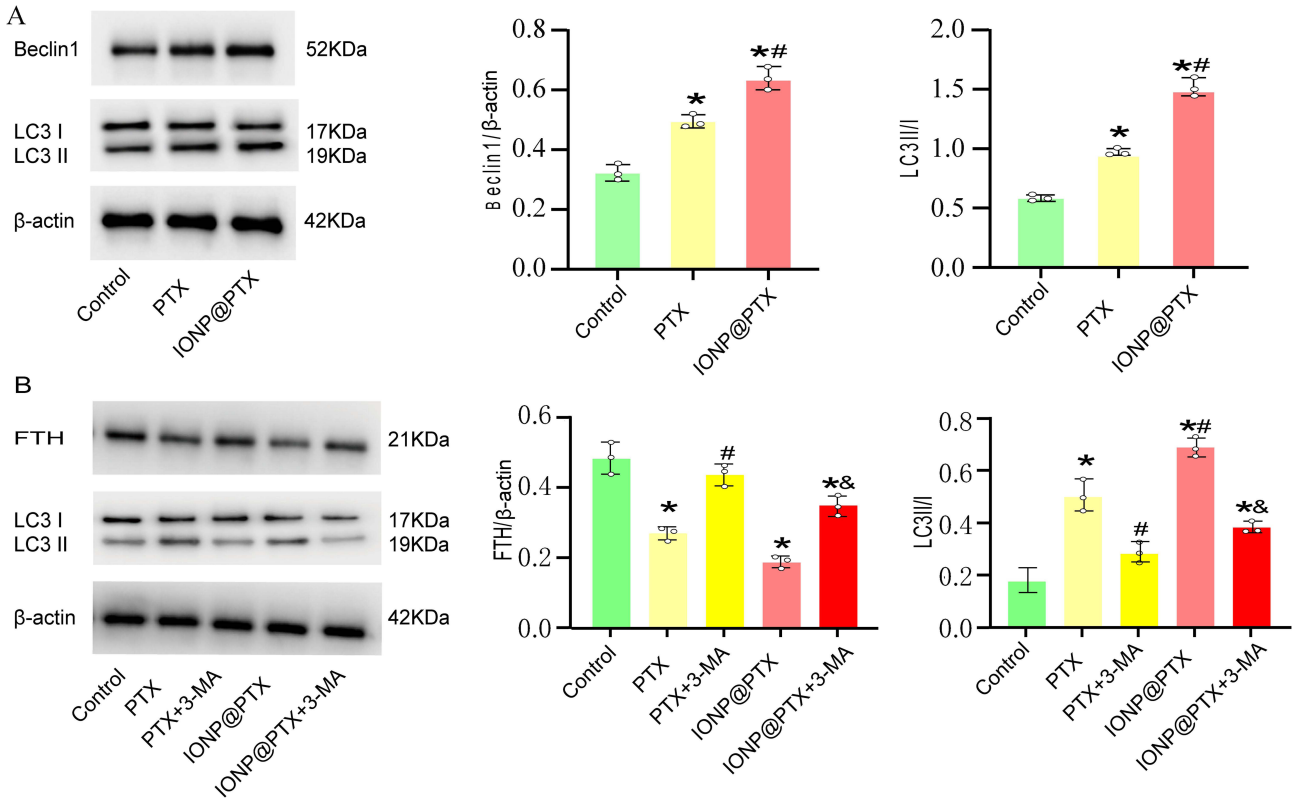

Figure 8 Determination of Beclin1, LC3II/I, FTH proteins in A549 cells by Western blot. (**A**) Representative images and relative levels expression of autophagy-related Beclin1, and LC3II/I proteins; (**B**) Representative images and relative levels expression of autophagy-related LC3II/I, and FTH proteins. Error lines were from triplicate runs. *P < 0.05, compared with control; #P < 0.05, compared with PTX group; &P < 0.05, compared with IONP@PTX group.

Abbreviations: IONP, iron oxide nanoparticles; PTX, paclitaxel; ROS, reactive oxygen species; LPD, lipid peroxidation; 3-MA, 3-methyladenine.

https://doi.org/10.2147/CMAR.S497238

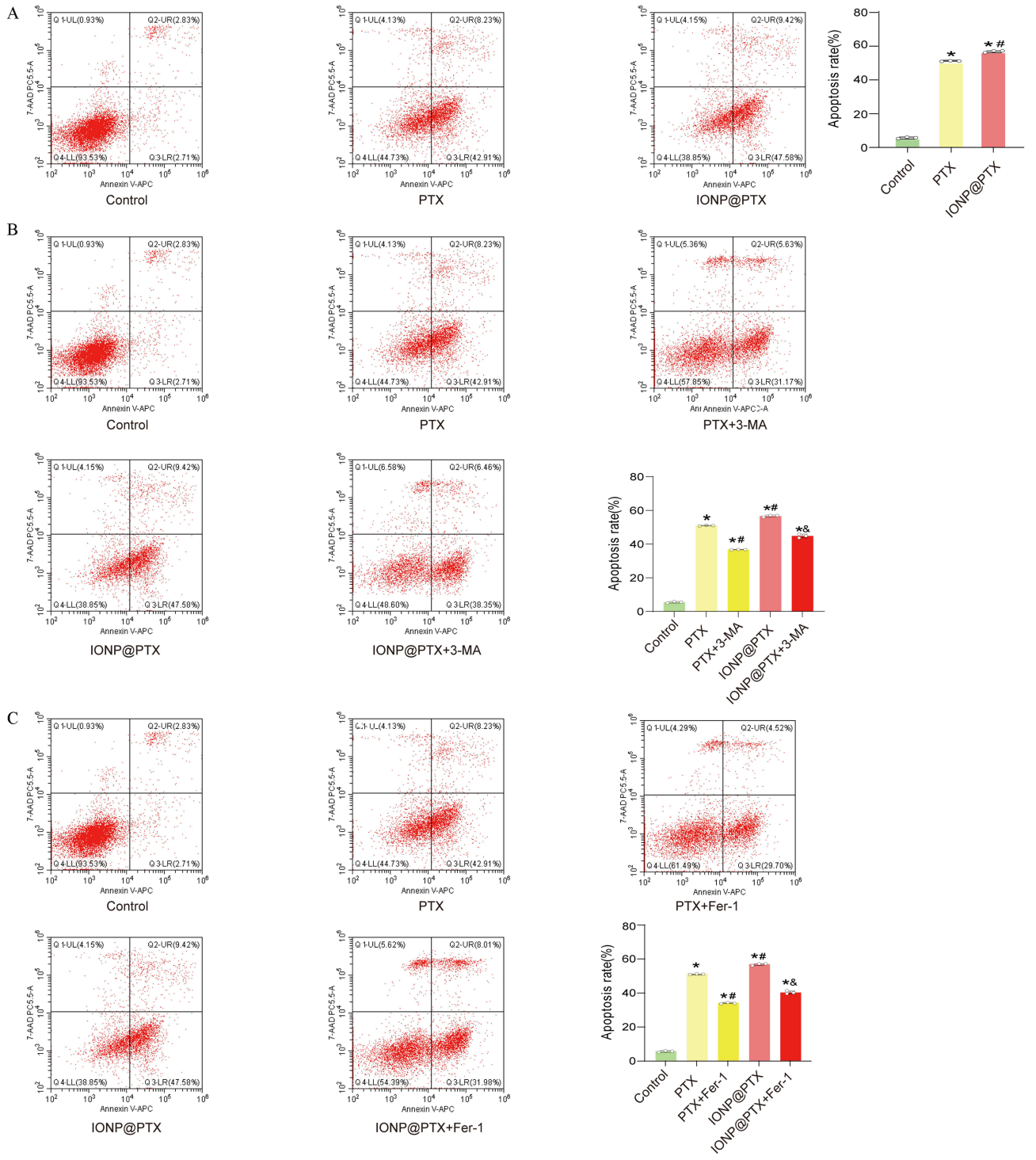

Figure 9 Induction of IONP@PTX on cell apoptosis by flow cytometry. (**A**) Representative flow diagram of apoptosis in A549 cells treated with single PTX, and IONP@PTX; (**B**) Apoptosis rates of A549 cells treated with single PTX, IONP@PTX, a combination of PTX with 3-MA, and a combination of IONP@PTX with 3-MA; (**C**) Representative flow diagram of apoptosis in A549 cells treated with PTX, a combination of PTX with ferrostatin-1, IONP@PTX, and a combination of IONP@PTX with ferrostatin-1.

Abbreviations: IONP, iron oxide nanoparticles; PTX, paclitaxel; 3-MA, 3-methyladenine; Fer-1, ferrostatin-1.

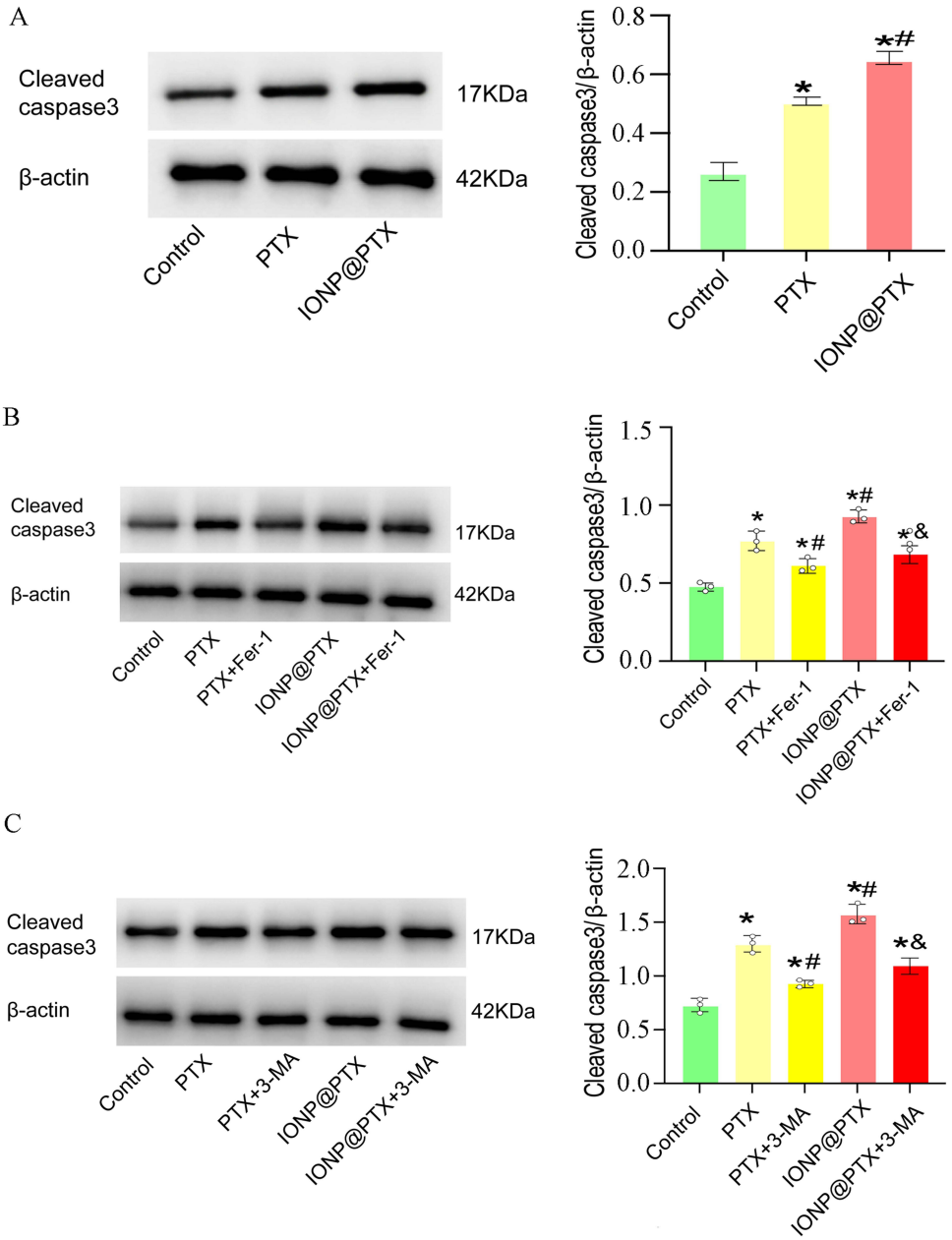

Figure 10 Determination of Cleaved caspase-3-related proteins by Western blot. (**A**) Representative images and relative expression level of Cleaved caspase-3-related protein in A549 cells treated with PTX or IONP@PTX; (**B**) Representative images and relative expression of Cleaved caspase-3 protein in A549 cells treated with PTX, IONP@PTX, a combination of PTX with ferrostatin-1, and a combination of IONP@PTX with ferrostatin-1; (**C**) Representative images and relative expression of Cleaved caspase-3 protein in A549 cells treated with PTX, IONP@PTX, a combination of PTX with 3-MA, and a combination of IONP@PTX with 3-MA.
Abbreviations: IONP, iron oxide nanoparticles; PTX, paclitaxel; 3-MA, 3-methyladenine; Fer-1, ferrostain-1.

Discussion

Accumulating evidence has confirmed that IONP may serve as a potent drug delivery vehicle to assist in the administration of PTX and work in concert with cancer cells.[13,14,25] In our current study, the successfully manufactured IONP@PTX, with a uniform particle size, good dispersion, stability, high encapsulation rate, and drug loading capacity, exhibited marked inhibitory effects on NSCLC.

Earlier work from our group and others have identified autophagy-dependent ferroptosis pathway induced by several kinds of nanoparticles.[1,14,15,24] Autophagy is an intracellular process of self-degradation and recirculation, which encapsulates proteins or organelles in the cytoplasm into a double-membrane structure termed an "autophagosome",

https://doi.org/10.2147/CMAR.S497238

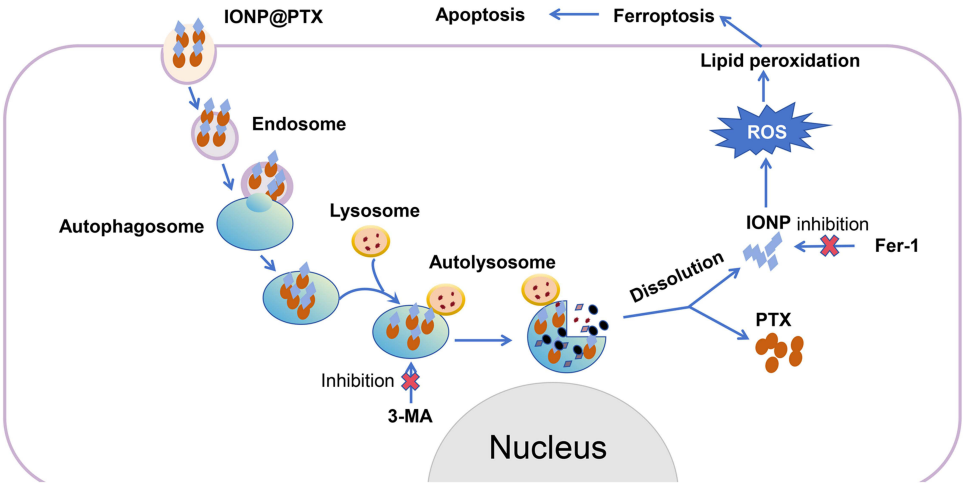

Figure 11 Schematic diagram of the potential mechanism underlying the inhibitory effects of IONP@PTX paclitaxel-loaded iron oxide nanoparticles on non-small cell lung cancer.
Abbreviations: IONP, iron oxide nanoparticles; PTX, paclitaxel; 3-MA, 3-methyladenine;Fer-1, ferrostatin-1.

which then fuses with lysosomes to form autophagic lysosomes and degrade the encapsulated contents.[26] During the autophagy, its marker LC3 is transformed from the cytoplasmic LC3-I form to the lipidated LC3-II form, thereby the magnitude of the LC3-II/I ratio can be used to estimate the level of autophagy. Identically, the Beclin1 protein interacts with several binding partners of the autophagy process as well as with regulatory proteins of the apoptotic cell death pathway, thus playing a crucial role in regulating the crosstalk between these two forms of cell death and leading to a wide range of physiological and pathophysiological conditions.[27] In our previous studies, IONP@PTX significantly increased the LC3-II/I ratio and the expression levels of Beclin1 protein in human glioma U251 and M059K cells together with SCLC NCI-H446 cell line compared with PTX.[13,14] Our present results further indicate that IONP@PTX induces autophagy in A549 cells to a greater extent and additional autophagy inhibitor 3-MA decreased both autophagy flux and cell death.

Apoptosis, also known as programmed cell death, is a highly conserved physiological mechanism that involves two fundamental pathways: the extrinsic or receptor-mediated pathway and the intrinsic or mitochondrial pathway.[28,29] Several factors, known pro-apoptotic proteins, play a critical role in the process of apoptosis.[30] Cleaved caspase-3 as an apoptosis inducer contributes to natural product dehydrocurvulari-induced apoptosis and significantly inhibited the growth of gastric tumors.[31] Our in vitro studies showed that IONP@PTX resulted in a significant up-regulation of Cleaved caspase-3 compared with the control and PTX groups. Interestingly, additional 3-MA or ferrostatin-1 decreased the levels Cleaved caspase-3 protein. Collectively, IONP@PTX may induce apoptosis in A549 cells via the autophagy pathway.

Ferroptosis is a novel type of programmed cell death that differs from apoptosis due to the iron-dependent accumulation of lipid peroxide,[32] and an aberrant build-up of lipid hydroperoxides in turn causes ferroptosis.[32,33] The lipophilic antioxidant ferritin, which is composed of heavy and light ferritin chains, regulates iron metabolism by sequestering and storing iron in a non-toxic and bioavailable form, thereby preventing harmful oxidative reactions.[34] Growing evidence indicates that, compared with normal tissues, the expression levels of FTH are significantly elevated in a variety of cancer types (eg, liver hepatocellular carcinoma, cholangiocarcinoma, and head and neck squamous cell carcinoma), involving in the regulation of ferroptosis.[35–37] In the present study, total iron ion concentration, intracellular levels of ROS and LPD significantly increased in the IONP@PTX group compared with PTX group, which was also supported by our previous findings on glioblastoma U251 and M059K cells, and SCLC NCI-H446,[13,14] suggesting that IONP@PTX induces ferroptosis in A549 cells. Notably, ferritin heavy chain 1(ferritin heavy chain 1) has been shown to attenuate ferroptosis and inhibit lipid peroxidation in pulmonary fibrosis.[38] Similarly, our experimental study of A549 cells indicated that ferrostatin-1 attenuated IONP@PTX-induced ferroptosis. GPX4 is one of the glutathione peroxidases

known to regulate ferroptosis via suppressing iron-dependent ROS and iron-dependent lipid peroxidation chain reaction in different cancer cell types.[39,40] Except for GPX4 in the regulation of lipid biosynthesis, ACSL4 is a pivotal enzyme responsible for the initiation of ferroptosis,[41] and SLC7A11, an amino acid counter transporter protein on the cell surface, is critical in preventing iron-induced apoptosis by inhibiting lipid peroxidation.[34,42] After incubation of A549 cells with our synthesized IONP@PTX, a remarkable elevated ACSL4 protein and lowered levels of GPX4 and SLC7A11 proteins were detected in our current study. Accumulating evidence indicates that erastin, sulfasalazine, and sorafenib's pharmacological suppression of SLC7A11 markedly reduced intracellular glutathione content, which in turn caused lipid peroxidation and ferroptosis.

Increasing evidence suggests that ferroptosis requires an autophagic mechanism to execute, and that excessive autophagy and lysosomal activity can promote ferroptosis, as characterized by significant iron accumulation and LPD.[43] It has been shown that autophagy mediates the degradation of ferritin and leads to ferroptosis caused by autophagic degradation of cellular FTH.[44,45] Ultrasmall iron oxide nanoparticles can induce ferroptosis, which is regulated through the Beclin 1/ATG 5-dependent autophagy pathway.[46] Similarly, IONP@PTX induced ferroptosis through the autophagy ferroptosis-dependent pathway in the human SCLS NCI-H446 and brain malignant glioblastoma M059K cells.[13] Autophagy, in turn, can promote the release of iron ions from IONP@PTX, leading to excessive intracellular ROS production and cell ferroptosis.[14] Recent studies have demonstrated that activation of ferroptosis is indeed dependent on the induction of autophagy.[34] Collectively, these results suggest that IONP@PTX-induces ferroptosis occurs via the ROS-mediated autophagy pathway in A549 cells.

Although the two genetic phenotypes and modes of death, ferroptosis and apoptosis, are distinct, there have been a growing number of conclusions proposing an association between them, and it has recently been confirmed that ferroptosis inhibitory protein 1, previously known as an apoptosis-inducing factor, synergistically triggers ferroptosis in conjunction with GPX4 inhibitors.[40] Furthermore, inactivation of GPX4 not only accelerates the progression of ferroptosis, but also sensitizes cells to apoptosis and necrotic apoptosis.[34] In light of recent studies, ferroptotic agents including artemisinin and artesunate induce C/EBP homologous protein via endoplasmic reticulum stress, promote p53 upregulated modulator of apoptosis, and potentially augment tumor necrosis factor-related apoptosis-inducing ligand (TRAIL)-induced apoptosis, thereby generating a synergistic effect of ferroptosis inducers with TRAIL to promote apoptosis.[47] Accordingly, we further speculate that IONP@PTX causes apoptosis through the ROS-mediated autophagy-dependent ferroptosis pathway and described in Figure 11. In brief, IONP@PTX enters the cells through the receptor mediated endosomes. After that, autophagosomes fuse with lysosomes to form autolysosomes in the final step of autophagy pathway, through which iron ions are released from IONP@PTX, leading to accumulation of intracellular ROS and cell ferroptosis, and by the ferroptosis can affect cell apoptosis. However, in vivo studies of IONP@PTX together with migration and invasion in vitro following the additional 3-MA or ferrostatin-1 are needed to verify the validity of this hypothesis.

Conclusion

IONP@PTX induces ferroptosis and apoptosis in A549 cells by upregulating autophagic processes.

Abbreviations

NSCLC, Non-small cell lung cancer; IONP@PTX, Iron oxide nanoparticles coated with paclitaxel; CCK-8, Cell Counting Kit-8; LPD, Lipid peroxidation; ROS, Reactive oxygen species; PTX, Paclitaxel; IONP, Iron oxide nanoparticles; FDA, Food and Drug Administration; GPX4, Glutathione peroxidase 4; GSH, Glutathione; FBS, Fetal bovine serum; OD, Optical density; ACSL4, Acyl–coenzyme A (CoA) synthetase long-chain family member 4; FTH, Ferritin heavy chain; SLC7A11, Solute carrier family 7 member 11; Fer-1, Ferrostatin-1; 3-MA, 3-methyladenine.

Data Sharing Statement

The datasets used and/or analyzed during the current study are available from the corresponding author on reasonable request.

Ethics Approval and Consent to Participate

This study complies with the Declaration of Helsinki.

Author Contributions

All authors made a significant contribution to the work reported, whether that is in the conception, study design, execution, acquisition of data, analysis and interpretation, or in all these areas; took part in drafting, revising or critically reviewing the article; gave final approval of the version to be published; have agreed on the journal to which the article has been submitted; and agree to be accountable for all aspects of the work.

Funding

The content of the funding section has been modified as follows: This work was supported by Project No. (2023GXNSFAA6385, AB0167, AB6017), the National Natural Science Foundation of China (grant no. 30228), Guangxi Key Laboratory of Big Data Intelligent Cloud Management for Neurological Diseases (grant no. ZTJ0005), Guangxi Medical and health key cultivation discipline construction project.

Disclosure

Rongchu Deng and Guanghong Liang are co-first authors for this study. The authors declare that they have no competing interests in this work.

References

1. Abdulbaqi IM, Assi RA, Yaghmur A, et al. Pulmonary delivery of anticancer drugs via lipid-based nanocarriers for the treatment of lung cancer: an update. *Pharmaceuticals*. 2021;14(8):725. doi:10.3390/ph0725
2. Clark SB, Alsubait S. Non-small cell lung cancer. 2023. *Barw Med J*. 2024;PMID: 35978.
3. Soffietti R, Abacioglu U, Baumert B, et al. Diagnosis and treatment of brain metastases from solid tumors: guidelines from the European Association of Neuro-Oncology (EANO). *Neuro Oncol*. 2017;19(2):162–174. doi:10.1093/neuonc/now241
4. Zhu L, Chen L. Progress in research on paclitaxel and tumor immunotherapy. *Cell Mol Biol Lett*. 2019;24:40. doi:10.1186/s1658-019-0164-y
5. Sharifi-Rad J, Quispe C, Patra JK, et al. Paclitaxel: application in modern oncology and nanomedicine-based cancer therapy. *Oxid Med Cell Longev*. 2021;2021:37700. doi:10.1155/2021/37700
6. Kampan NC, Madondo MT, McNally OM, et al. Paclitaxel and its evolving role in the management of ovarian cancer. *Biomed Res Int*. 2015;2015:43076. doi:10.1155/2015/43076
7. Horwitz SB. Personal recollections on the early development of taxol. *J Nat Prod*. 2004;67(2):136–138. doi:10.1021/np4464
8. Schiff PB, Horwitz SB. Taxol stabilizes microtubules in mouse fibroblast cells. *Proc Natl Acad Sci U S A*. 1980;77(3):1561–1565. doi:10.1073/pnas.77.3.1561
9. Zhou YS, Wang W, Chen N, et al. Research progress of anti-glioma chemotherapeutic drugs (Review). *Oncol Rep*. 2022;47(5):101. doi:10.3892/or.2022.8312
10. Zhang Y, Zhai M, Chen Z, et al. Dual-modified liposome codelivery of doxorubicin and vincristine improve targeting and therapeutic efficacy of glioma. *Drug Deliv*. 2017;24(1):1045–1055. doi:10.1080/17544.2017.14334
11. Dessai A, Nayak UY, Nayak Y. Precision nanomedicine to treat non-small cell lung cancer. *Life Sci*. 2024;346:12614. doi:10.1016/j.lfs.2024.12614
12. Mali P, Sherje AP. Cellulose nanocrystals: fundamentals and biomedical applications. *Carbohydr Polym*. 2022;275:18668. doi:10.1016/j.carbpol.2021.18668
13. Nie Q, Chen W, Zhang T, et al. Iron oxide nanoparticles induce ferroptosis via the autophagic pathway by synergistic bundling with paclitaxel. *Mol Med Rep*. 2023;28(4):198. doi:10.3892/mmr.2023.13085
14. Chen H, Wen J. Iron oxide nanoparticles loaded with paclitaxel inhibits glioblastoma by enhancing autophagy-dependent ferroptosis pathway. *Eur J Pharmacol*. 2022;921:14860. doi:10.1016/j.ejphar.2022.14860
15. Yoneshima Y, Morita S, Ando M, et al. Phase 3 trial comparing nanoparticle albumin-bound paclitaxel with docetaxel for previously treated advanced NSCLC. *J Thorac Oncol*. 2021;16(9):1523–1532. doi:10.1016/j.jtho.2021.03.027
16. Liu F, Li L, Lan M, et al. Psoralen-loaded polymeric lipid nanoparticles combined with paclitaxel for the treatment of triple-negative breast cancer. *Nanomedicine*. 2021;16(27):2411–2430. doi:10.2217/nnm-2021-0241
17. Diab T, Alkafaas SS, Shalaby TI, et al. Paclitaxel nanoparticles induce apoptosis and regulate txr1, cyp3a4 and cyp2c8 in breast cancer and hepatoma cells. *Anticancer Agents Med Chem*. 2020;20(13):1582–1591. doi:10.2174/1241530
18. Qi J, Jin F, Xu X, et al. Combination cancer immunotherapy of nanoparticle-based immunogenic cell death inducers and immune checkpoint inhibitors. *Int J Nanomed*. 2021;16:1435–1456. doi:10.2147/IJN.S5999
19. Xu Y, Wu H, Huang J, et al. Probing and enhancing ligand-mediated active targeting of tumors using sub-5 nm ultrafine iron oxide nanoparticles. *Theranostics*. 2020;10(6):2479–2494. doi:10.7150/thno.39560
20. Mou Y, Wang J, Wu J, et al. Ferroptosis, a new form of cell death: opportunities and challenges in cancer. *J Hematol Oncol*. 2019;12(1):34. doi:10.1186/s3045-019-0720-y
21. Huang S, Cao B, Zhang J, et al. Induction of ferroptosis in human nasopharyngeal cancer cells by cucurbitacin B: molecular mechanism and therapeutic potential. *Cell Death Dis*. 2021;12(3):237. doi:10.1038/s1419-021-03516-y

22. Wang S, Luo J, Zhang Z, et al. Iron and magnetic: new research direction of the ferroptosis-based cancer therapy. *Am J Cancer Res*. 2018;8 (10):1933–1946. PMID: 36846.
23. Stockwell BR. Ferroptosis turns 10: emerging mechanisms, physiological functions, and therapeutic applications. *Cell*. 2022;185(14):2401–2421. doi:10.1016/j.cell.2022.06.003
24. Rakesh R, PriyaDharshini LC, Sakthivel KM, et al. Role and regulation of autophagy in cancer. *Biochim Biophys Acta Mol Basis Dis*. 2022;1868 (7):16400. doi:10.1016/j.bbadis.2022.16400
25. Aftab S, Shah A, Nadhman A, et al. Nanomedicine: an effective tool in cancer therapy. *Int J Pharm*. 2018;540(1–2):132–149. doi:10.1016/j.ijpharm.2018.02.007
26. Debnath J, Gammoh N, Ryan KM. Autophagy and autophagy-related pathways in cancer. *Nat Rev mol Cell Biol*. 2023;24(8):560–575. doi:10.1038/s1580-023-00585-z
27. Prerna K, Dubey VK. Beclin1-mediated interplay between autophagy and apoptosis: new understanding. *Int J Biol Macromol*. 2022;204:258–273. doi:10.1016/j.ijbiomac.2022.02.005
28. Xu X, Lai Y, Hua ZC. Apoptosis and apoptotic body: disease message and therapeutic target potentials. *Biosci Rep*. 2019;39(1):BSR0992. doi:10.1042/BSR0992
29. Carneiro BA, El-Deiry WS. Targeting apoptosis in cancer therapy. *Nat Rev Clin Oncol*. 2020;17(7):395–417. doi:10.1038/s1571-020-0341-yE
30. Zakariah M, Molele RA, Mahdy MAA, et al. Regulation of spermatogenic cell apoptosis by the pro-apoptotic proteins in the testicular tissues of mammalian and avian species. *Anim Reprod Sci*. 2022;247:17158. doi:10.1016/j.anireprosci.2022.17158
31. Xu H, Shen X, Li X, et al. The natural product dehydrocurvularin induces apoptosis of gastric cancer cells by activating PARP-1 and caspase-3. *Apoptosis*. 2023;28(3–4):525–538. doi:10.1007/s0495-023-01811-x
32. Grube J, Woitok MM, Mohs A, et al. ACSL4-dependent ferroptosis does not represent a tumor-suppressive mechanism but ACSL4 rather promotes liver cancer progression. *Cell Death Dis*. 2022;13(8):704. doi:10.1038/s1419-022-05137-5
33. Dodson M, Castro-Portuguez R, Zhang DD. NRF2 plays a critical role in mitigating lipid peroxidation and ferroptosis. *Redox Biol*. 2019;23:11107. doi:10.1016/j.redox.2019.11107
34. Kang R, Tang D. Autophagy and ferroptosis - What's the connection? *Curr Pathobiol Rep*. 2017;5(2):153–159. doi:10.1007/s0139-017-0139-5
35. Fang X, Cai Z, Wang H, et al. Loss of cardiac ferritin H facilitates cardiomyopathy via slc7a11-mediated ferroptosis. *Circ Res*. 2020;127 (4):486–501. doi:10.1161/CIRCRESAHA.120.36509
36. Mumbauer S, Pascual J, Kolotuev I, et al. Ferritin heavy chain protects the developing wing from reactive oxygen species and ferroptosis. *PLoS Genet*. 2019;15(9):e8396. doi:10.1371/journal.pgen.18396
37. Du J, Wang X, Li Y, et al. DHA exhibits synergistic therapeutic efficacy with cisplatin to induce ferroptosis in pancreatic ductal adenocarcinoma via modulation of iron metabolism. *Cell Death Dis*. 2021;12(7):705. doi:10.1038/s1419-021-03996-y
38. Sun Y, Ren Y, Song LY, et al. Targeting iron-metabolism: a potential therapeutic strategy for pulmonary fibrosis. *Biomed Pharmacother*. 2024;172:16270. doi:10.1016/j.biopha.2024.16270
39. Kim JW, Min DW, Kim D, et al. GPX4 overexpressed non-small cell lung cancer cells are sensitive to RSL3-induced ferroptosis. *Sci Rep*. 2023;13 (1):8872. doi:10.1038/s1598-023-35978-9
40. Bersuker K, Hendricks JM, Li Z, et al. The CoQ oxidoreductase FSP1 acts parallel to GPX4 to inhibit ferroptosis. *Nature*. 2019;575 (7784):688–692. doi:10.1038/s1586-019-1705-2
41. Miao Z, Tian W, Ye Y, et al. Hsp90 induces Acsl4-dependent glioma ferroptosis via dephosphorylating Ser637 at Drp1. *Cell Death Dis*. 2022;13 (6):548. doi:10.1038/s1419-022-04997-1
42. Chen X, Bi H, Zhang M, et al. Research of sleep disorders in patients with acute cerebral infarction. *J Stroke Cerebrovasc Dis*. 2015;24 (11):2508–2513. doi:10.1016/j.jstrokecerebrovasdis.2015.06.033
43. Zhou B, Liu J, Kang R, et al. Ferroptosis is a type of autophagy-dependent cell death. *Semin Cancer Biol*. 2020;66:89–100. doi:10.1016/j.semcancer.2019.03.002
44. Gao M, Monian P, Pan Q, et al. Ferroptosis is an autophagic cell death process. *Cell Res*. 2016;26(9):1021–1032. doi:10.1038/cr.2016.95
45. Hou W, Xie Y, Song X, et al. Autophagy promotes ferroptosis by degradation of ferritin. *Autophagy*. 2016;12(8):1425–1428. doi:10.1080/18627.2016.17366
46. Wen J, Chen H, Ren Z, et al. Ultrasmall iron oxide nanoparticles induced ferroptosis via Beclin1/ATG5-dependent autophagy pathway. *Nano Converg*. 2021;8(1):10. doi:10.1186/s0580-021-00260-z.
47. Lee YS, Lee DH, Choudry HA, et al. Ferroptosis-induced endoplasmic reticulum stress: cross-talk between ferroptosis and apoptosis. *mol Cancer Res*. 2018;16(7):1073–1076. doi:10.1158/1541-7786.MCR-18-0055